Energy Advances

ROYAL SOCIETY OF CHEMISTRY

PAPER

View Article Online
View Journal

Cite this: DOI: 10.1039/d6ya00067c

A novel vanadium–titanium redox flow battery with a mixed electrolyte approach

Chivukula Kalyan Sundar Krishna and Yansong Zhao *

Redox flow batteries (RFBs) enable independent scaling of energy and power, making them a suitable candidate for grid-scale energy storage solutions. However, the market is currently dominated by vanadium RFBs, which are prone to extreme price volatility. To reduce the inherent material costs while retaining the efficiencies, the study investigates a novel vanadium–titanium RFB using (i) a separate, acid-based system (V_2O_5 + H_2SO_4 catholyte, and $TiCl_3$ + HCl anolyte) (system-1), (ii) a premixed acid-based electrolyte at 0% state of charge (system-2), and (iii) an ionic-liquid-based premixed electrolyte comprising [Bmim]Cl + VCl_3 and its titanium counterpart (system-3). Several physical and electrochemical characterization studies were performed, such as viscosity and density measurements from 298 to 333 K, cyclic voltammetry tests, and electrochemical impedance spectroscopy to establish a stable redox window for V(IV/V) and Ti(III/IV) in the presence of an ionic-liquid. In galvanostatic cycling with a SPEEK membrane, system-1 delivers coulombic efficiency (CE) greater than 98%, at 10–20 mA cm^{-2}, with an energy density of 24.53 Wh L^{-1}. System-2 (premixed acid) retains the CE%, while the voltage efficiency (VE) drops by 10%. The results demonstrated that premixing at 0% SOC effectively limits the crossover in V–Ti RFBs, while optimization of proton donors and the inclusion of additives are necessary to enhance the nominal discharge potential.

Received 6th March 2026,
Accepted 5th April 2026

DOI: 10.1039/d6ya00067c

rsc.li/energy-advances

Introduction

The global transition toward low-carbon energy systems has significantly increased the interest in grid-scale energy storage technologies that can effectively manage fluctuations in renewable power generation. Among the various emerging electrochemical energy storage technologies, redox flow battery batteries (RFBs) play a crucial role due to their numerous advantages over traditional metal-ion batteries, of which, the decoupling of energy and power density places them at the forefront.[1–8] This unique ability to store the energy in the liquid electrolyte by means of electrochemical redox reactions amongst the redox active materials, rather than the electrodes inside the battery, significantly aids in expanding the horizons in grid-scale energy storage, due to their scalability and reusability. Of the various contenders in the RFB technology, vanadium redox flow batteries (VRFBs) are currently leading in the marketspace of commercially available flow battery technologies on a grid-scale basis as compared to several other component combinations such as V–Fe, Fe–Cr, Fe–Zn, Zn–Br, Mn-based, and Ce-based flow batteries.[9–24] The presence of vanadium in various oxidation states (+2 to +5) in the catholyte and anolyte solutions serves as a medium to eliminate the risk of cross-contamination during the breakage of the ion-exchange membrane, which is lacking in the other flow battery technologies. Moreover, a traditional VRFB exhibits a low theoretical open-circuit potential (OCP) of 1.26 V, which limits its implementation in several applications, where Li-ion batteries (LIBs) prevail. However, this has been targeted by numerous researchers around the globe in an effort to achieve a flow battery with high OCP while utilizing low-cost and non-toxic materials. In this regard, several RFBs have been developed by incorporating a novel catholyte or an anolyte redox active species, consisting of a higher reduction potential, such as Mn, Fe, and Ce as opposed to V^{4+}/V^{5+} (1 V *vs.* SHE).[12–15,22,25–29] Owing to its natural abundance, chemical stability, and relatively high standard electrode potential of 1.5 V *vs.* SHE, manganese has been widely employed as a catholyte material in combination with numerous anolyte solutions. Along these lines, zinc has been employed as an anolyte, yielding a zinc–manganese redox flow battery (ZMRFB) with a theoretical open-circuit potential (OCP) of approximately 2.2 V, as reported by Liu *et al.*[20] The study showcased that the incorporation of glycine enhanced the binding energy of the Gly–Mn^{2+} complex compared to that of Mn^{2+}–H_2O, thereby suppressing Mn-based precipitate formation and significantly improving the cycling stability and overall energy efficiency of the ZMRFB system.

Building upon the advantages of manganese, particularly its high redox potential, abundance, and lower cost as compared to vanadium, Dong *et al.*[24] introduced a manganese–titanium

Department of Safety, Chemistry and Biomedical Laboratory Sciences, Western Norway University of Applied Sciences (HVL), 5063, Bergen, Norway.
E-mail: yansong.zhao@hvl.no, yansong.zhao2004@gmail.com

mixed-electrolyte redox flow battery (MTRFB) that achieved an open-circuit potential (OCP) of 1.6 V, and an energy density of 23.5 Wh L^{-1}, suggesting the effectiveness of utilizing titanium as a potential anolyte solution in a RFB. Furthermore, a recent study by Ahmed *et al.*[30] highlights the advantages of titanium as a redox-active material, stating that its natural abundance is nearly '50' times greater than vanadium, and its global production is about '100' times higher along with a lower material cost *viz.* 1/10th of vanadium. Combined with a low material cost and high abundance, titanium represents a promising low-cost alternative for anolyte development in RFBs. However, the utilization of various combinations of the anolyte and catholyte presents an imminent challenge of 'electrolyte-mixing'. Along these lines of incorporating alternative anolytes while preventing cross-contamination, Zeng *et al.*[17] introduced a novel lead–iron redox flow battery (Pb–Fe RFB), employing Pb/Pb^{2+} and Fe^{2+}/Fe^{3+} as the anolyte and catholyte solutions, respectively. The RFB exhibited an OCP of 0.9 V, which, although significantly lower as compared to that of alkaline Zn–Fe RFBs,[31] demonstrated favourable electrochemical performance. Furthermore, the key strategy employed in their study was the implementation of a pre-mixed electrolyte approach to mitigate the issues in relation to the electrolyte crossover, which is pertinent to several RFB technologies. Prior to initiating charge–discharge cycling, the Fe and Pb-based electrolytes were pre-mixed at 0% state of charge (SOC) and subsequently divided into equal volumes to serve as the anolyte and catholyte solutions, respectively. This strategy effectively minimized concentration imbalances and improved long-term stability of the flow battery. The optimized Pb–Fe RFB delivered CE% of 96.2% and 98.2%, and EE% of 86.2% and 73.5% at discharge current densities of 40 mA cm^{-2} and 120 mA cm^{-2}, respectively. Following the same pre-mixing concept, the authors later developed a cadmium–iron (Cd–Fe) RFB,[10] utilizing Cd^{2+}/Cd^{0} as the anolyte, and Fe^{2+}/Fe^{3+} as the catholyte solution. Although the Cd^{2+}/Cd^{0} couple (0.4 V *vs.* SHE) provides a higher reduction potential than V^{2+}/V^{3+} (0.26 V *vs.* SHE), the toxicity and environmental hazards associated with cadmium require stringent handling precautions. Despite these concerns, the Cd–Fe RFB exhibited excellent electrochemical performance, achieving a CE of 98.7%, an EE of 80.2% at 120 mA cm^{-2}, and an outstanding capacity retention of 99.87% over extended cycles of operation. These studies collectively underscore the effectiveness of electrolyte pre-mixing prior to RFB operation in maintaining charge balance, suppressing crossover, and improving the long-term electrochemical stability of the RFB system. However, the incorporation of lead and cadmium along with iron and vanadium, respectively, depicts a hybrid RFB, rather than a complete one. In this regard, utilizing a pre-mixed electrolyte approach, a novel RFB has been developed by utilizing vanadium (V^{4+}/V^{5+}) as the catholyte solution due to its well-known advantage of relatively high OCP as compared to Fe-based systems, and titanium (Ti^{3+}/Ti^{4+}) as the anolyte due to its abundance and reversibility, and thereby minimizing the material procurement costs.

However, due to the presence of different anolyte and catholyte solutions, there is an imminent threat of electrolyte cross-mixing, which will be addressed in the manuscript, by utilizing a pre-mixed electrolyte approach at 0% SOC, and dividing the solution into two equal halves to function as catholyte and anolyte solution. Furthermore, in order to encourage the implementation of green-chemistry, ionic liquid named 1-butyl 3-methyl imidazolium chloride (BmimCl) has been utilized in the pre-mixed electrolyte approach in combination with vanadium chloride (VCl_3),[32] along with an acid-based system comprising vanadium pentoxide (V_2O_5) in diluted sulphuric acid solution (H_2SO_4), for comparative performance. Moreover, to reduce to the overall cost of operation, the Nafion membrane has been replaced with SPEEK, as membrane plays a crucial role in determining the economics of the flow battery setup on a large-scale.

A couple of electrochemical tests such as the cyclic voltammetry (CV) and electrochemical impedance spectroscopy (EIS) tests were conducted to evaluate the stability window and to assess the electrolyte's resistance in relation with the viscosity of the electrolyte along with numerous cyclic charge–discharge tests. These studies provided an in-depth understanding of the working of a novel pre-mixed vanadium–titanium redox flow battery, and its implementation at the grid-scale by replacing the vanadium based anolyte solutions, thereby reducing the material procurement costs and extending the overall life cycle while maintaining the stability.

Physical and electrochemical performance

Prior to evaluating the electrochemical performance of the V–Ti RFB utilizing the pre-mixed electrolyte approach, the electrolytes have been synthesized and mixed at 0% SOC, and the corresponding dynamic viscosities and densities have been measured with the help of a rolling ball viscometer, over a range of temperatures *viz.* 25 °C to 50 °C. The forward and backward run time measurements have been noted, and the experiments have been conducted till the variation coefficient is less than 0.1%, to obtain an accurate result. As the viscosity of the liquid electrolytes plays a crucial role in determining the pumping costs, mass-transport resistances, and the pressure build-up inside the RFB setup, it is indeed essential to utilize an electrolyte with lower dynamic viscosities. Fig. 1(a) and (b) depict the obtained results for the pre-mixed ionic liquid based system and acid-based system over a range of temperatures, respectively.

It can be derived from the obtained results that the dynamic viscosities of the pre-mixed systems lie below 5 mPa s with a density greater than 1.1 g cm^{-3} at room temperature, suggesting optimal physical behaviour necessary for an electrolyte.[33] Subsequent to the evaluation of the physical properties of the pre-mixed electrolyte system, CV and EIS tests have been conducted to obtain a stable operating window, and the resistances offered by the electrolyte region. Since the acid-based electrolyte (system-1) has been illustrated in an earlier manuscript, this section details the pre-mixed ionic liquid and pre-mixed acid based systems (2, and 3). As illustrated in Fig. 2, CV tests have been performed between the limits of −0.65 V to 1.2 V with reference to the 'Ag/AgCl' electrode, and system-3 showcased appreciable stability for more than 100 cycles of operation at a scan rate of 0.1 V sec^{-1}.

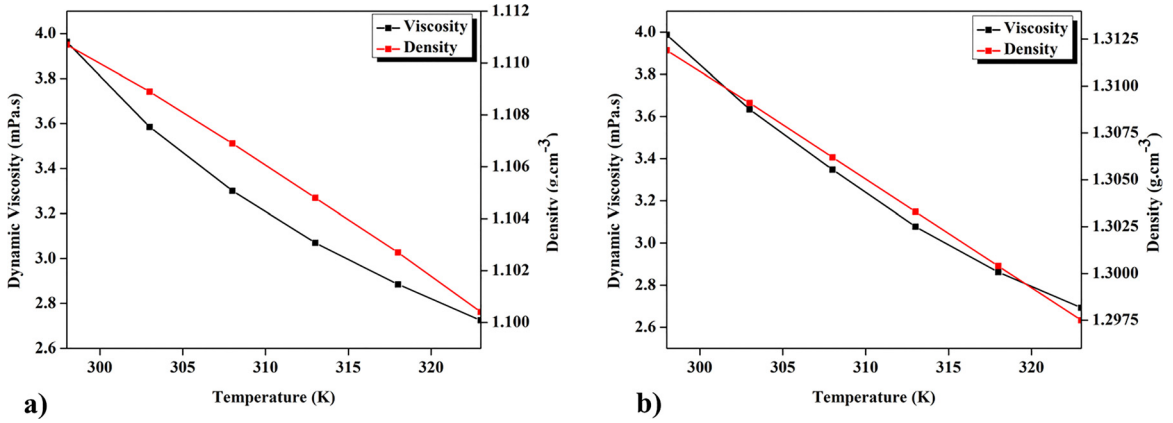

Fig. 1 Dynamic viscosity and density variation with temperature from 298 K to 333 K for the pre-mixed ionic liquid (system-3) (a), and pre-mixed acid-based (system-2) solutions (b).

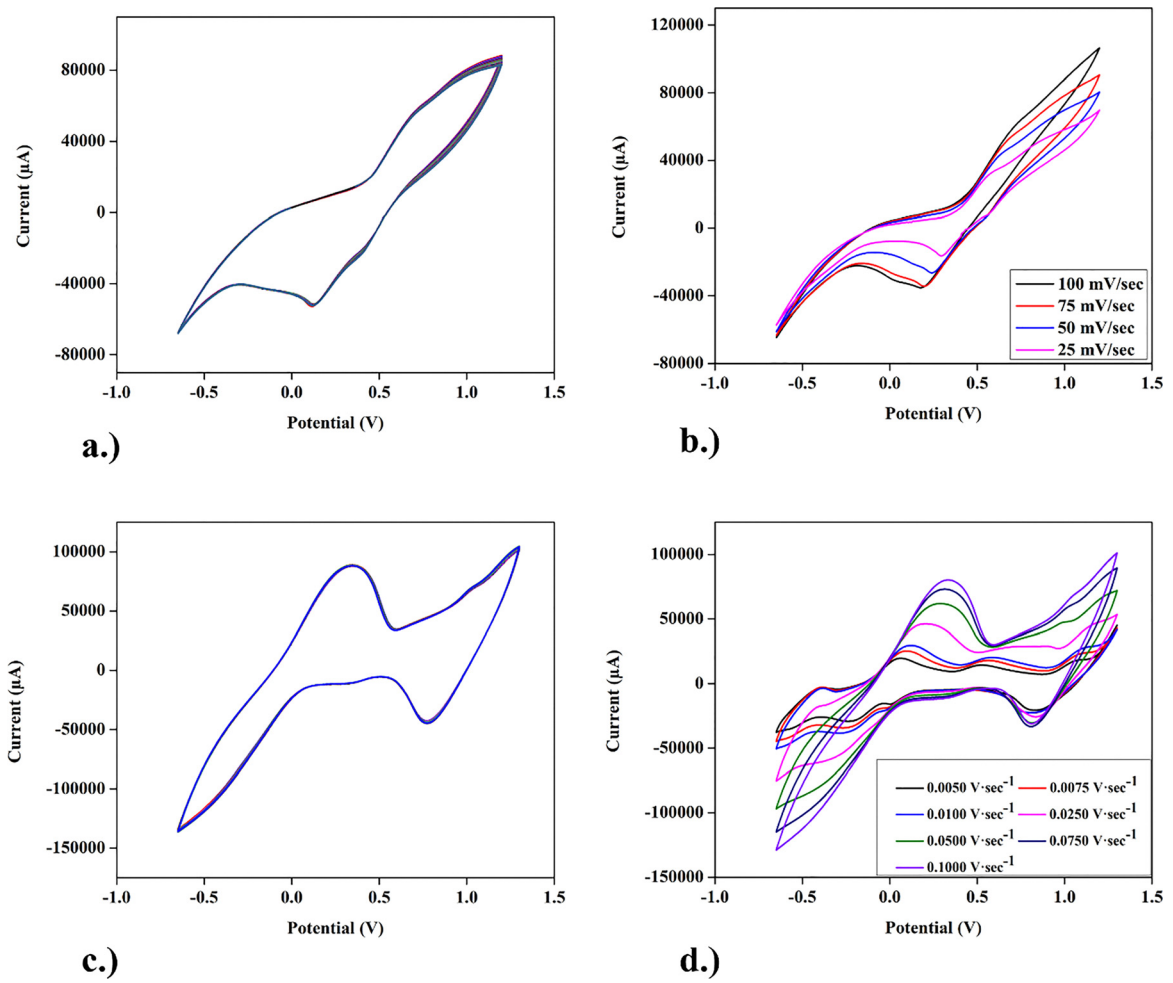

Fig. 2 Cyclic voltammetry tests conducted for the pre-mixed ionic liquid (system-3) (a) and (b) and pre-mixed acid (system-2) (c) and (d) based electrolytes at a fixed scan rate of 0.1 V sec^{-1} (a), at varying scan rates ranging from 0.1 V sec^{-1} to 0.025 V sec^{-1} (b), cyclic stability at a scan rate of 0.075 V sec^{-1} (c), and at varying scan rates ranging from 0.005 V sec^{-1} to 0.1 V sec^{-1} (d) with the help of a 3-electrode setup utilising 'Ag/AgCl' as the reference, and 'Pt' as the counter electrodes.

Moreover, the presence of oxidation and reduction peaks is illustrated in Fig. 2, wherein the peak at the higher voltage range *viz.* greater than 0.5 V suggests the conversion of V^{4+} to V^{5+}, and the small peak in the reduction indicates the reduction of V^{5+}. Similarly, the peaks obtained around 0 V and in the negative potential region indicate the oxidation and reduction

of Ti^{3+}/Ti^{4+}, and *vice versa*. Due to the existence of a negative potential as compared to the reference electrode Ag/AgCl (0.4 V *vs.* SHE), the redox reactions of vanadium exist in the positive potential region, and titanium exists in the negative region, suggesting a flow battery comprising of an ionic liquid-based electrolyte (system-3) capable of showcasing a well-defined kinetics over numerous cycles of operation, with a wide electrochemical potential window, and an OCP of approximately 0.9 V.

Furthermore, as visualised in Fig. 2(c), the pre-mixed acid-based system showcased impressive stability over 100 cycles, along with a well-defined redox potential. On utilizing the obtained CV graphs for system-2 and 3, the peak currents have been plotted with the square root of scan rates, and a linear relation has been obtained, signifying a diffusion-controlled mechanism with R^2 values of 0.9839 and 0.9945, respectively, allowing the implementation of the Randles–Sevcik equation to obtain their diffusion coefficients, and thereby the Nicholson method to obtain the heterogeneous electron transfer rate constants. On evaluating the peak currents, *i.e.*, cathodic and anodic, at various scan rates, the diffusion coefficients have been evaluated as,

$$I_p = \left(2.69 \times 10^5\right) n^{\frac{3}{2}} A D^{\frac{1}{2}} C v^{\frac{1}{2}},$$

where 'I_p' denotes the peak current, 'n' is the electron transfer, 'A' is the active surface area of the electrode, while 'D' denotes the diffusion coefficient, 'C' represents the concentration of the electrolyte solution, and 'v' is the scan rate. Utilizing the above-mentioned expression, the diffusion coefficients can be evaluated as,

$$D = \left(\frac{m}{2.69 \times 10^5 n^{\frac{3}{2}} AC}\right)^2,$$

where 'm' is the slope obtained from I_p *vs.* $v^{\frac{1}{2}}$. The obtained values of diffusion coefficients have been illustrated in Table 1, along with their rate constants evaluated as,

$$k_0 = \psi \left(\frac{\pi D n F v}{RT}\right)^{\frac{1}{2}},$$

where 'ψ' was evaluated utilizing the respective peak separations obtained from the CV graph at various scan rates. The kinetic parameter has been evaluated as,

$$\psi = \frac{-0.6288 + 0.0021 \Delta E_P}{1 - 0.017 \Delta E_P}.$$

As evident from the obtained data, the progress from system 1 to 3 leads to a significant reduction in the kinetic parameters accompanied by an increase in the dynamic viscosity of the liquid electrolyte, thereby negatively affecting the electrochemical performance of the mixed electrolyte systems by offering an increase in the resistances. However, as compared to system 1, system 2 showcased similar kinetics, suggesting competitive performance metrics. However, as evident from 'ΔE_p', none of the 3 systems portray an ideal reversible behaviour with degradation towards system 3. The combination of slow mass transport and sluggish electron kinetics – suggesting a less reversible redox couple – showcases a large overpotential even at modest currents, thereby a drastic reduction in the VE%. As the surface electrochemical reactions are governed by the Butler–Volmer (BV) equation, the exchange current density denoted by (J_0) depends on the rate constant. Therefore, to maintain a fixed current discharge condition, a lower rate constant (system 3 – as compared to systems 1 and 2) elevates the overpotential of the system to meet the prescribed discharging conditions. The relationship between electrode current density (J) and overpotential (η) can be described as follows:

$$J = J_0 \left\{ \exp\left[\frac{\alpha_a z F}{RT}(\eta)\right] - \exp\left[-\frac{\alpha_c z F}{RT}(\eta)\right] \right\},$$

where the terms 'z', 'F', 'R', and 'T' denote the electrons involved in the redox reactions, Faraday constant, universal gas constant, and absolute temperature, respectively. Furthermore, the exchange current density denoted by 'J_0' can be evaluated as,

$$J_0 = zFk^0 C_0^{(1-\alpha)} C_R^{\alpha},$$

where the rate constant (k^0) governs 'J_0'. As explained earlier, to retain a similar discharge current amongst systems 2 and 3, due to a decrement in the rate constant along with the diffusion coefficient as compared to system 1, the overpotential requirement rises, leading to a drastic drop in the nominal discharge potential assisted by sluggish redox reactions and bulk diffusion of ionic species. Consequently, VE% showcases a greater drop as compared to system 2, and the following will be visualized in the upcoming section of the manuscript.

Subsequent to the stability and kinetic analysis of the pre-mixed systems, EIS studies have been performed to evaluate the resistances offered by the electrolyte region, and the obtained results are depicted in Fig. 3.

As illustrated in Fig. 3, the pre-mixed liquid electrolyte showcases a solution resistance closer to 5.75 Ω and a charge-transfer resistance of 1.2 Ω, respectively, measured w.r.t to OCP at room temperature, wherein the pre-mixed acid-based system demonstrates a lower solution resistance of ~2.2 Ω. Due to a lower dynamic viscosity offered by the electrolyte region as illustrated in Fig. 1, the solution and the charge-transfer resistances of the electrolyte region have been reduced, as compared

Table 1 A comparison of diffusion coefficients and rate constants of systems 2 and 3 with respect to system 1

System	Averaged diffusion coefficient ($cm^2\ s^{-1}$)	Averaged rate constant ($cm\ s^{-1}$)	ΔE_p (mV)
Separate vanadium–titanium (system 1)	3.2×10^{-6}	2×10^{-4}	216–363
Mixed electrolyte with acid (system 2)	3.0×10^{-6}	1×10^{-4}	249–380
Mixed ionic liquid (system 3)	9.8×10^{-7}	1×10^{-5}	370–510

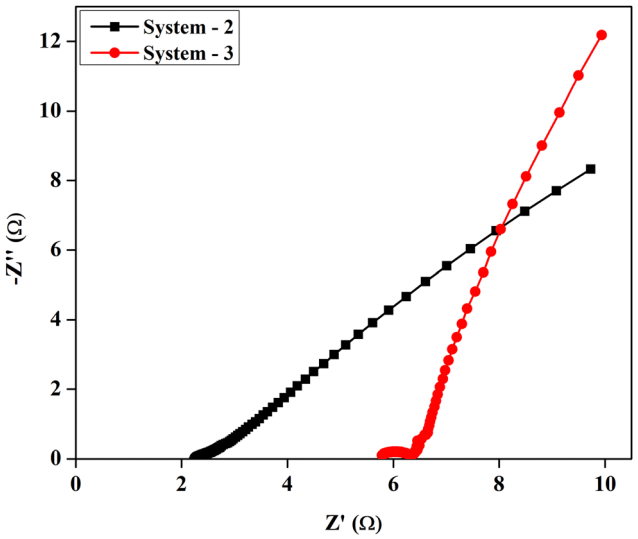

Fig. 3 Electrochemical impedance spectroscopy tests conducted for the pre-mixed ionic liquid (system-3) and pre-mixed acid (system-2) based electrolyte with the help of a 3-electrode setup utilising Ag/AgCl as the reference, and Pt as the counter electrodes at an AC potential perturbation of 5 mV amplitude and over a frequency range of 0.1 Hz to 200 kHz.

to a separate traditional ionic-liquid based system.[32] However, the imminent problem of the lack of H^+ ions necessary to facilitate the charge–discharge of the RFB persists in the ionic-liquid-based system, as compared to the acid-based one, which will be explored in the upcoming section.

Charge–discharge behaviour

Prior to evaluating the electrochemical charge–discharge performance and thereby the efficiencies of the V–Ti pre-mixed electrolyte approach method, the RFB comprising $V_2O_5 + H_2SO_4$ in deionized water as the catholyte and $TiCl_3$ + HCl in aqueous solution as the anolyte were utilized along with a SPEEK membrane (system-1) to compare the metrics and analyse the performance at a similar discharge current, charge capacity, and voltage range.

As depicted in Fig. 4, the V–Ti RFB showcased an impressive performance, with a CE%, VE, and EE% greater than 98%, 60%, and 60%, respectively, at a discharge current of 10 mA cm^{-2}, and 98%, 55%, and 55%, respectively, at a discharge current of 20 mA cm^{-2}.

Furthermore, the synthesized electrolytes exist in a completely charged state, *i.e.*, the catholyte comprising the 'V^{+5}' state and the anolyte utilizing 'Ti' in its +3 oxidation state, allowing the V–Ti RFB to discharge prior to charging (a consequence of residual charge, and not an electrochemical artifact) which can be visualised in Fig. 4(b)–(d). As illustrated in Fig. 4(d), at a charging capacity of 0 mAh, the discharge capacity of the V–Ti RFB showcased a value of 125.89 mAh at a nominal discharge potential of 0.8914 V. However, from the subsequent cycles of operation, the charge–discharge test proceeded in a steady fashion, as depicted in Fig. 4(a), (b), and (d). At a higher discharging current of 20 mA cm^{-2}, as opposed to 10 mA cm^{-2}, the nominal discharge potential dropped by approximately 0.12 V, which is due to an increase in the ohmic drop; however, the CE% remained steady over 98–99%, suggesting negligible capacity fade due to crossover, in the presence of the SPEEK membrane as illustrated by the obtained CE%.

Subsequently, the 2nd cycle of operation, as depicted in Fig. 4(a), and (d), involved charging the RFB until the charging current fell below 10 mA cm^{-2} at a charging voltage of 1.3 V, to assess the overall energy density of the flow battery. The charging capacity corresponded to 410.36 mAh with a discharge capacity of 406.23 mAh, at a CE% of 98.99%, yielding an energy density of $24.53_{\text{w.r.t. catholyte or anolyte}}$ Wh L^{-1}.

Following the analysis of the electrochemical performance of V–Ti RFB utilizing system-1 as the basis, the pre-mixed electrolyte approach has been utilized as a precaution to avoid cross-mixing of catholyte and anolyte solutions (system-2). Unlike system-1 utilizing 'V^{+5}' and 'Ti^{+3}', the RFB utilizing system-2 consists of the anolyte and catholyte at a 0% SOC due to the presence of 'V^{+5}' and 'Ti^{+3}' in both the electrolytes leading to zero driving force for the flow of electrons, suggesting that the battery needs to be charged prior to discharging. However, similar to system-1, the pre-mixed acid based solutions showcased an impressive CE% greater than 98%. As showcased in Fig. 5, the RFB utilizing a pre-mixed electrolyte approach showcased similar performance metrics at a discharging current of 10 mA cm^{-2}.

However, the average VE% and EE% have been reduced by approximately 10% *viz.* ~55% as opposed to ~65% at 10 mA cm^{-2}, during the charge–discharge performance of the battery, which can be corroborated to a decrease in the average rate constants and diffusion constants along with an increase in the dynamic viscosity. Prior to pre-mixing, the anolyte comprising '$TiCl_3$' + 'HCl' in DI water showcased a dynamic viscosity of 1.35 mPa s, as opposed to 3.9 mPa s, in the pre-mixed electrolyte approach at room temperature, along with a decrease in the average rate constants and diffusion coefficients as showcased in Table 1. This discrepancy in the obtained values might have led to an increase in the internal resistances, lowering the ionic conductivity and thereby inducing an enhanced ohmic drop and subsequently lowering the nominal discharge potential to 0.7717 V, as opposed to 0.9061 V, and thereby negatively impacting the VE% and EE%. In comparison with system-1, the pre-mixed acid-based system demonstrated comparable performance in terms of CE% but lacked in terms of VE% due to an increase in the ohmic resistances, leading to a drop in the nominal discharging potential. The gradual drop in the VE% and EE% until the 19th cycle can be correlated to an increase in the internal resistances and discharging current densities, leading to an ohmic drop. During repeated charge–discharge cycles, changes in the electrolyte composition and concentration distribution might have occurred leading to hindrance caused by accumulation of ions near the electrode surfaces and across the membrane over the due course of cycling. These changes can slightly increase the resistance to the ion transport and the overpotential required for the redox reactions. As a result, the difference between the charging voltage and

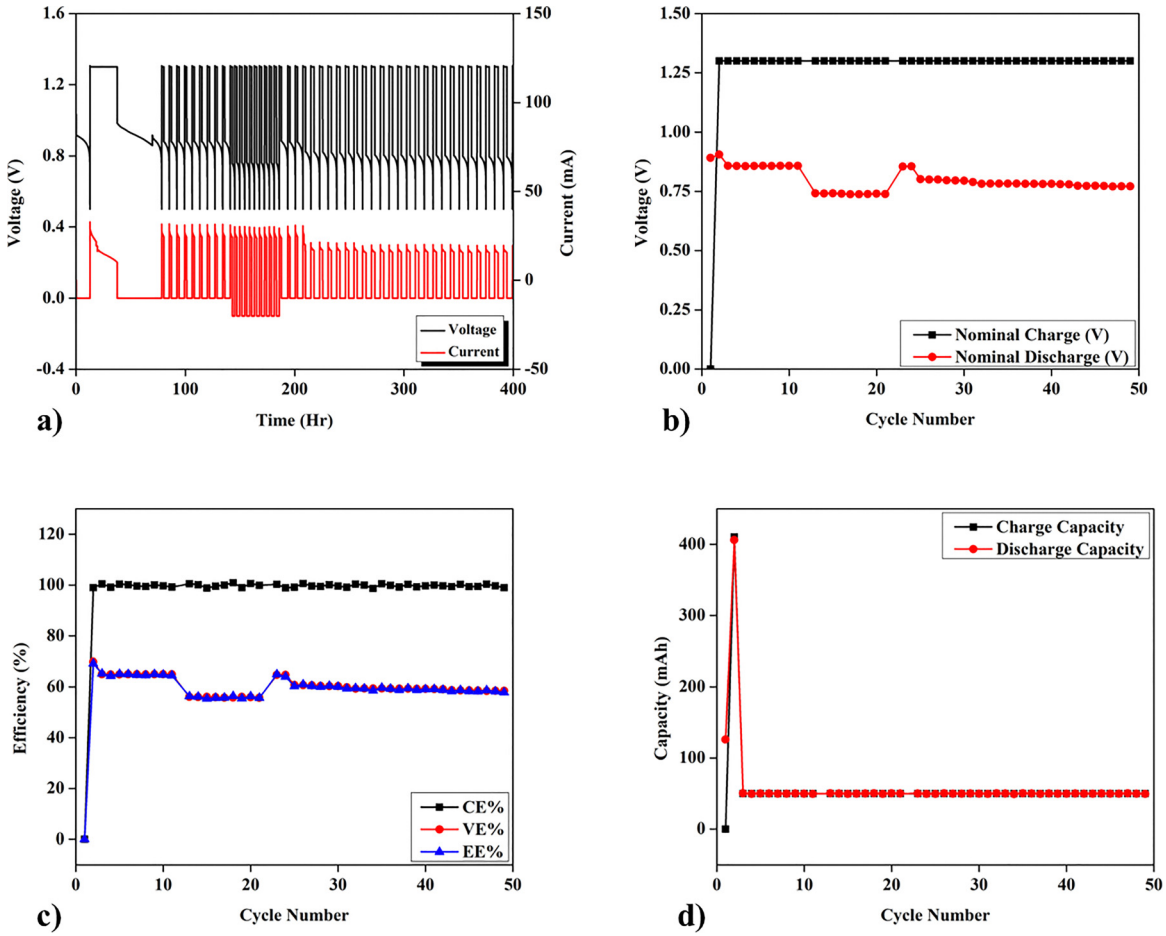

Fig. 4 Charge–discharge behaviour of V–Ti RFB utilizing separate acid based electrolytes (system-1) as the basis charged till 1.3 V and discharged at current densities corresponding to 10 mA cm^{-2} and 20 mA cm^{-2} (a) with its nominal charging and discharging voltages (b) along with the efficiencies (CE%,VE%, and EE%'s) (c) and charge–discharge capacity variation (d) for 50 cycles of operation.

discharging voltage becomes larger, incurred by a rise in the drop due to the overpotential, causing a decrement in the nominal discharge voltage,[33–35] leading to a constant decrease in the VE% during the initial cycling, prior to achieving a steady-state condition *viz.* the 20th cycle of operation, as evident from the obtained results.

In a similar fashion, minor crossover or slight imbalances in the oxidation states of vanadium and titanium species in the complex pre-mixed electrolyte setup may develop over time, as evident from a decrement in the CE%. These effects can prevent a small fraction of the active species from fully participating in the electrochemical reactions within the fixed voltage range used during cycling, leading to a slow decrease in discharge capacity.

Furthermore, unlike systems-1 and 2, system-3 utilises ionic-liquid (BmimCl) as the solvent and VCl_3 as the vanadium source rather than V_2O_5 in the presence of DI water, which has been explored in our previous studies involving the utilization of ionic liquids to enhance the solubility of vanadium based salts, and thereby promoting greener chemistry rather than utilizing a corrosive acid-based system.[32] The synthesized catholyte and anolyte solutions consists of vanadium in its '+4' oxidation state along with the titanium counterpart, unlike system-1, leading to a complete charging process prior to initializing a discharge. Similar to the earlier systems, the RFB has been charged till 50 mAh at a voltage of 1.3 V and discharged at a current of 10 mA cm^{-2} to comparatively analyse the performance.

As showcased in Fig. 6, the ionic liquid-based system showcased stable performance for numerous cycles of operation. However, as compared to the previous systems, system-3 showcased a reduction in the charging speed, due to a decrease in the 'H+' ion concentration, which can be inherently linked to the absence of an acid (H_2SO_4). As visualised in Fig. 6(b), and (c), the efficiency in the 1st cycle, *viz.* formation cycle, is higher as compared to the subsequent cycles. During the 1st cycle of operation, rather than implementing a fixed capacity restriction, the RFB has been allowed to charge till the charging current falls below 10 mA. During this charging regime, a capacity of ~110 mAh has been reached, and subsequently the charging protocol has been modified to a fixed charge capacity of 50 mAh to enable a consistent comparison of CE%/VE%/EE% under steady operating conditions. As VE% and EE% depend on polarization and SOC, the formation cycle, *viz.* 1st cycle, showed a difference in the obtained efficiencies as compared to the subsequent steady-state cycling.

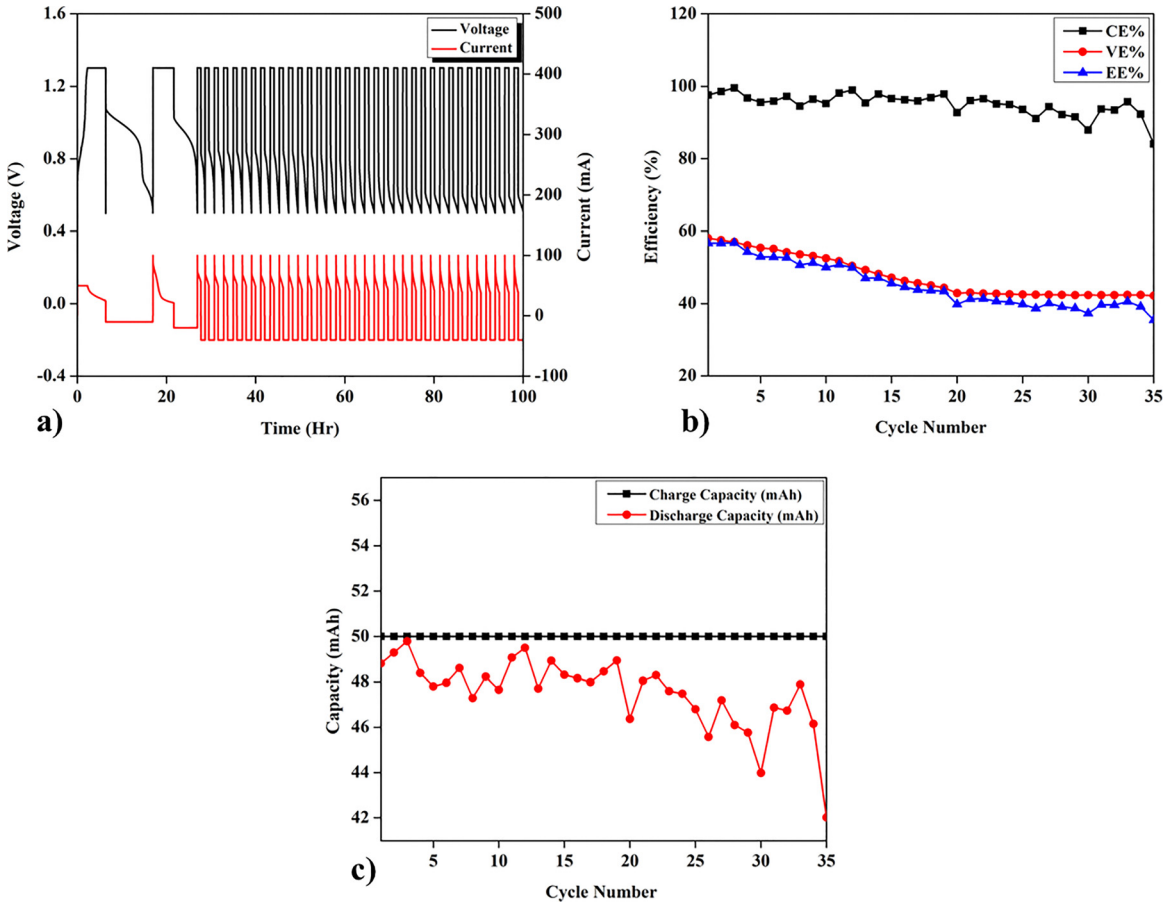

Fig. 5 Charge–discharge performance of V-Ti RFB utilizing the pre-mixed acid-based electrolyte (system-2) as the basis charged at 100 mA cm^{-2} till the voltage reaches 1.3 V (a), along with its efficiencies (CE%, VE%, and EE%'s) (b), and charge–discharge capacity variation (c) as a function of cycle number.

Furthermore, the RFB showcased a CE% greater than 90% as opposed to 98% during steady-state cycling, as compared to the earlier system, suggesting a minute crossover and undesirable side reactions. In the present electrolyte environment, the parasitic side reactions can include the evolution of chlorine gas, along with hydrogen and oxygen formation associated with water splitting. Such processes consume charge without contributing to useful energy output, thereby negatively impacting the overall CE%. Furthermore, literature studies have indicated that SPEEK and related sulfonated aromatic membranes have demonstrated oxidation-induced degradation, polymer backbone scission, swelling, crack formations, and micro-porosity in the presence of 'VO_2^+' medium, which may adversely affect the ionic transport properties and contribute to long-term capacity retention of the pre-mixed VTRFB setup.[33–35]

As compared to system-1, the ionic liquid-based system showcased a drastic drop in the VE%, and EE% *viz.* 20%, mainly due to a decrement in the rate constants and diffusion coefficients as evident from Table 2, along with an increase in the resistance of the electrolyte as illustrated earlier, and a lack of H+ ions to facilitate the necessary charge balance, in addition to the parasitic side reactions leading to the formation of chlorine gas.[32] Furthermore, in an effort to relate the physical and electrochemical characteristics along with their varying efficiencies, a comparative summary of the mixed electrolyte systems has been included in Table 2. As visualised from Table 2, system-3 has exhibited less favourable electrochemical characteristics as compared to system-2, including lower diffusion coefficients, heterogeneous electron-transfer rate constant, solution resistance, and a similar dynamic viscosity. This indicates that dynamic viscosity alone does not explain the difference between their VE% (between system-2 and 3); however, they are inherently higher as compared to system-1 *viz.* 1.35 mPa s[36] as opposed to 3.9 mPa s. However, system-3 has clearly demonstrated less favourable electrochemical characteristics as compared to system-1 and 2, as illustrated in Table 1; correspondingly, system-3 demonstrated a lower VE% and EE%, as compared to system-2, during the initial cycles of operation and similar values in later cycles.

Furthermore, in order to enhance the performance metrics of the pre-mixed electrolyte approach utilizing ionic liquids, additives are indeed necessary to facilitate the charge balance during the charging and discharging of the flow battery, along with the addition of environmentally friendly amino acid derivatives such as glycine to subside chlorine gas evolution,[20] thereby effectively enhancing the overall electrochemical performance of mixed V-Ti RFBs, which will be the primary focus of future works.

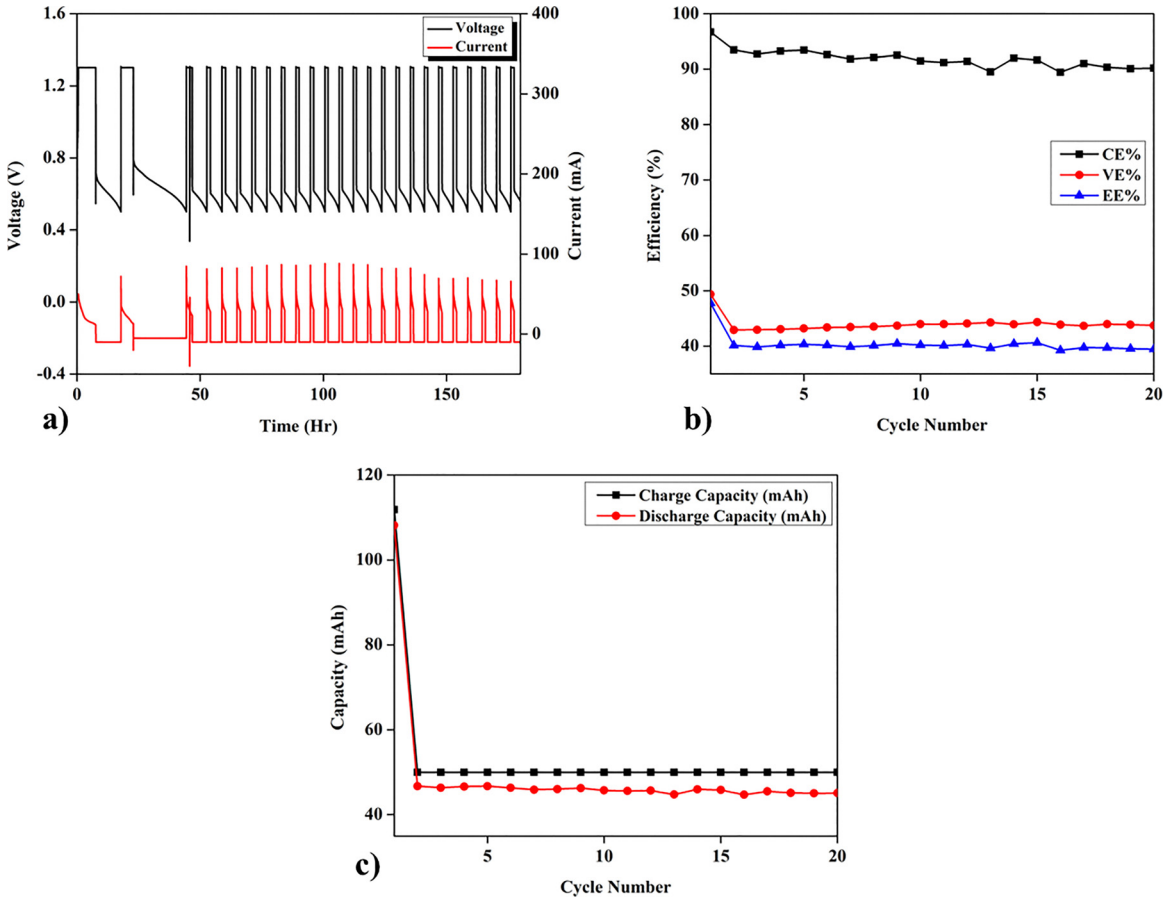

Fig. 6 Charge–discharge behaviour of the V–Ti RFB utilizing a pre-mixed ionic liquid based electrolyte (system-3) as the basis at 1.3 V charging until the capacity reaches 50 mAh, and discharging at 10 mA cm^{-2} (a), along with its efficiencies (CE%, VE%, and EE%'s) (b), and charge–discharge capacity (c) variation as a function of cycle number.

Table 2 A comparative analysis of the physical and electrochemical performance of pre-mixed acid based (system-2), and pre-mixed ionic liquid based electrolytes (system-3) along with explicit VE% and EE%

Parameters	Pre-mixed acid based electrolyte	Pre-mixed ionic liquid based electrolyte
Dynamic viscosity (at RT)	~3.9 mPa s	~3.9 mPa s
Average diffusion coefficients	3×10^{-6} cm^2 s^{-1}	9.8×10^{-7} cm^2 s^{-1}
Average heterogeneous rate constant	1×10^{-4} cm s^{-1}	1×10^{-5} cm s^{-1}
Solution resistance (R_s)	~2.2 Ω	~5.8 Ω
VE% (1st 10 cycles)	~55%	~43%
EE% (1st 10 cycles)	~52%	~39%
VE% (after 10 cycles)	40–45%	~43%

Experimental section

Materials and chemicals

Titanium chloride ($TiCl_3$), hydrochloric acid (HCl), vanadium pentoxide (V_2O_5), sulfuric acid (H_2SO_4), and hydrogen peroxide (H_2O_2) were utilized in the preparation of the anolyte and catholyte solutions, respectively, without further purification. Moreover, 1-butyl-3-methylimidazolium chloride (BmimCl) and vanadium chloride (VCl_3) were utilized to synthesize ionic-liquid-based catholyte solution. Moreover, commercially available SPEEK membranes were utilized along with graphite current collector plates and carbon felt electrodes.

Electrolyte preparation

The catholyte was prepared by dissolving 1 M (mol L^{-1}) V_2O_5 in an aqueous solution of 3 M H_2SO_4, 1 M H_2O_2 and deionized water at room temperature while stirring for approximately 4 hours. $TiCl_3$ has been mixed with 1 M HCl and DI water to synthesize anolyte solution. The preparation process of the

ionic-liquid based catholyte has been detailed in our earlier studies.[32] Furthermore, the synthesized solutions have been premixed to achieve a catholyte and an anolyte solution with 0% SOC.

Electrochemical characterization

Cyclic voltammetry (CV) measurements were conducted using a conventional three-electrode configuration connected to a potentiostat (Palmsens MultiTrace 4). A carbon felt electrode (1 cm^2) was employed as the working electrode, a platinum wire as the counter electrode, and an Ag/AgCl (3 M KCl) electrode served as the reference electrode. All measurements were carried out in 1 M solutions, prepared using analytical grade chemicals and deionized water. Prior to each experiment, the carbon felt working electrode was washed thoroughly with ethanol and deionized water and dried under ambient conditions. Cyclic voltammograms were recorded over an appropriate potential window (from −0.65 V to 1.2 V *vs.* Ag/AgCl for the ionic liquid-based pre-mixed electrolyte solution) at varying scan rates (25–100 mV s^{-1}). All measurements were performed at room temperature under an ambient atmosphere.

Furthermore, the same setup has been used while performing the electrochemical impedance spectroscopy (EIS) studies. The Palmsens MultiTrace 4 system has been utilized in this measurement, and the test was conducted over a frequency range of 0.1 Hz to 200 kHz with an AC potential perturbation of 5 mV amplitude, measured against the OCP.

Redox flow battery testing

A symmetric redox flow battery with different catholyte and anolyte solutions has been assembled, which comprised two pieces of graphite plates and carbon foam as the electrode with an active area of 1 cm^2 (1 cm × 1 cm). The flow rates of the catholyte and anolyte solutions have been fixed at 50% of the overall RPM of the pump, which corresponds to a mass flow rate of 0.54 g sec^{-1}. Furthermore, the volumes of the catholyte and anolyte solutions utilized were 15 mL each. The charge and discharge studies were evaluated utilizing LANHE-CT3002A (LANHE, Wuhan, China). Unless otherwise specified, the cut-off voltage was specified at 0.5 V for the discharge and 1.3 V during the charging process at a charge capacity of 50 mAh throughout this work.

Conclusion

This work systematically evaluates a novel V–Ti redox flow battery across three different electrolyte configurations, namely: (i) a separate acid-based V–Ti RFB with SPEEK as the baseline configuration, (ii) a pre-mixed acid-based system at 0% SOC, and (iii) a pre-mixed ionic-liquid based system. To benchmark the three different electrolyte systems in a uniform manner, their performance has been evaluated and compared on the basis of their efficiencies (CE%, VE%, and EE% values), nominal discharging voltages, rate transfer coefficients, diffusion coefficients, and dynamic viscosities along with their key advantages, major drawbacks, and practical applicability.

In this regard, system-1 (separate acid-based V–Ti RFB utilizing SPEEK) served as the electrochemical benchmark. It delivered a CE% greater than 98%, a VE% of about 65% at 10 mA cm^{-2}, and about 55% at 20 mA cm^{-2}, with a corresponding EE% close to the VE% values, and an energy density of 24.53 Wh L^{-1} on a single-electrolyte basis. In addition to these performance metrics, this system has demonstrated the highest nominal discharge voltage among the three different electrolyte configurations and the most favourable overall electrochemical behaviour – in terms of diffusion coefficients and heterogeneous rate transfer coefficients. Its major advantages are the high CE% *viz.* ∼98%, while utilizing a low-cost ion-exchange membrane (SPEEK) instead of Nafion. However, its main limitation is the distinct catholyte and anolyte regions, which are potentially at risk of cross-mixing during practical operations.

Furthermore, system-2 (premixed acid-based V–Ti RFB utilizing SPEEK) demonstrated that premixing at 0% SOC is a viable strategy to suppress crossover-related imbalance while still retaining a high CE% *viz.* ∼95%. However, as compared to system-1, the VE% and EE% decreased to about 55%, accompanied by a lower nominal discharge voltage during its initial cycles of operation. Based on the physical and electrochemical characterization studies provided in the manuscript, this reduction is consistent with less favourable transport and polarization behaviour, subsequent to the pre-mixing of liquid electrolytes at 0% SOC.

Nevertheless, amongst the mixed-electrolyte configurations studied here, system-2 has showcased balanced overall performance metrics because it preserved high coulombic efficiency while simplifying the electrolyte management and reducing the severity of cross-contamination concerns. Therefore, system-2 appears to exhibit the most practically promising configuration in the present work when both electrochemical performance and crossover tolerance are considered together.

In addition, system-3 (premixed ionic-liquid based V–Ti RFB with SPEEK) extended the concept of V–Ti RFB toward a greener and more compositionally flexible electrolyte design by incorporating an ionic-liquid named 'BmimCl' along with 'VCl_3' to serve as the vanadium based electrolyte. This system showed stable cycling over numerous cycles of operation and retained a CE% >90%; however, its VE% and EE% were lower as compared to the other systems *viz.* ∼43%, and ∼39%, respectively. This reduction has been attributed to less favourable electrochemical characteristics including slower rate transfer and diffusion coefficients along with lower proton availability for charge balance. The main advantage of system-3 lies in the feasibility of utilizing a pre-mixed green ionic liquid incorporated electrolyte as an alternative to the traditional corrosive acid-based electrolyte, at a penalty incurred in VE% and EE%. However, in its current form, system-3 is therefore better interpreted as a platform for future electrolyte optimization rather than an immediately competitive benchmark.

Together, the three-system comparison clarifies the main contribution of this study from a broader perspective. First, it establishes a viable V–Ti chemistry with SPEEK, as a workable non-VRFB platform capable of achieving high CE% while

greatly reducing the dependence on vanadium and Nafion, and thereby improving economics – due to the volatile costs of vanadium resources. Secondly, it demonstrates that premixing at 0% SOC can be utilized as a practical strategy to mitigate crossover-related imbalances caused in V–Ti systems, although this benefit is accompanied by a trade-off in VE% and EE%.

Overall, the present results indicate that the premixed acid-based system (system-2) offers the most balanced performance by demonstrating a high CE% and potentially limiting the crossover related issues within the tested mixed-electrolyte configurations, whereas the ionic-liquid based system (system-3) represents a long-term route toward greener, sustainable, and compositionally tuneable V–Ti RFBs. Future improvement should therefore focus on increasing the nominal discharge voltage and VE% through electrolyte modifications, proton-donor and additive optimization, and mitigation of parasitic side reactions.

Conflicts of interest

There are no conflicts to declare.

Data availability

Data are available as request for the article.

Acknowledgements

The authors acknowledge Western Norway University of Applied Sciences for financial support to this R&D project.

References

1 M. Winter and R. J. Brodd, What are batteries, fuel cells, and supercapacitors?, *Chem. Rev.*, 2004, **104**(10), 4245–4269.
2 N. Nitta, F. Wu, J. T. Lee and G. Yushin, Li-ion battery materials: Present and future, *Mater. Today*, 2015, **18**(5), 252–264.
3 J. B. Goodenough and K. S. Park, The Li-ion rechargeable battery: A perspective, *J. Am. Chem. Soc.*, 2013, **135**(4), 1167–1176.
4 B. Dunn, H. Kamath and J. M. Tarascon, Electrical energy storage for the grid: A battery of choices, *Science*, 2011, **334**(6058), 928–935.
5 J. B. Goodenough and Y. Kim, Challenges for rechargeable Li batteries, *Chem. Mater.*, 2010, **22**(3), 587–603.
6 B. E. Conway, Transition from ''Supercapacitor'' to ''Battery'' Behavior in Electrochemical Energy Storage, *J. Electrochem. Soc.*, 1991, **138**(6), 1539–1548.
7 A. González, E. Goikolea, J. A. Barrena and R. Mysyk, Review on supercapacitors: Technologies and materials, *Renewable Sustainable Energy Rev.*, 2016, **58**, 1189–1206.
8 C. Liu, F. Li, M. Lai-Peng and H. M. Cheng, Advanced materials for energy storage, *Adv. Mater.*, 2010, **22**(8), E28–E62.
9 A. Okazawa, T. Kakuchi, K. Kawai and M. Okubo, Iron-based catholytes for aqueous redox-flow batteries, APL, *Materials*, 2023, **11**(11), 110901.
10 Y. K. Zeng, T. S. Zhao, X. L. Zhou, L. Wei and H. R. Jiang, A low-cost iron-cadmium redox flow battery for large-scale energy storage, *J. Power Sources*, 2016, **330**, 55–60.
11 L. Zhang, H. Zhang, Q. Lai, X. Li and Y. Cheng, Development of carbon coated membrane for zinc/bromine flow battery with high power density, *J. Power Sources*, 2013, **227**, 41–47.
12 P. K. Leung, C. Ponce de León and F. C. Walsh, An undivided zinc–cerium redox flow battery operating at room temperature (295 K), *Electrochem. Commun.*, 2011, **13**(8), 770–773.
13 P. K. Leung, M. R. Mohamed, A. A. Shah, Q. Xu and M. B. Conde-Duran, A mixed acid based vanadium–cerium redox flow battery with a zero-gap serpentine architecture, *J. Power Sources*, 2015, **274**, 651–658.
14 P. Silambarasan, A. G. Ramu, M. Govarthanan, W. Kim and I. S. Moon, Cerium-polysulfide redox flow battery with possible high energy density enabled by MFI-Zeolite membrane working with acid-base electrolytes, *Chemosphere*, 2022, **291**(1), 132680.
15 D. Reynard, S. Maye, P. Peljo, V. Chanda, H. H. Girault and S. Gentil, Vanadium-Manganese Redox Flow Battery: Study of Mn(III) Disproportionation in the Presence of Other Metallic Ions, *Chemistry*, 2020, **26**(32), 7250–7257.
16 K. S. Archana, S. Suresh, P. Ragupathy and M. Ulaganathan, Investigations on new Fe–Mn redox couple based aqueous redox flow battery, *Electrochim. Acta*, 2020, **345**, 136245.
17 Y. K. Zeng, T. S. Zhao, X. L. Zhou, L. Wei and Y. X. Ren, A novel iron-lead redox flow battery for large-scale energy storage, *J. Power Sources*, 2017, **346**, 97–102.
18 M. Nan, L. Qiao, Y. Liu, H. Zhang and X. Ma, Improved titanium-manganese flow battery with high capacity and high stability, *J. Power Sources*, 2022, **522**, 230995.
19 M. Ulaganathan, S. Suresh, K. Mariyappan, P. Periasamy and R. Pitchai, New Zinc–Vanadium (Zn–V) Hybrid Redox Flow Battery: High-Voltage and Energy-Efficient Advanced Energy Storage System, *ACS Sustainable Chem. Eng.*, 2019, **7**(6), 6053–6060.
20 Y. Liu, M. Nan, Z. Zhao, B. Shen, L. Qiao, H. Zhang and X. Ma, Manganese-based flow battery based on the MnCl2 electrolyte for energy storage, *Chem. Eng. J.*, 2023, **465**, 142602.
21 L. Qiao, C. Xie, M. Nan, H. Zhang, X. Ma and X. Li, Highly stable titanium–manganese single flow batteries for stationary energy storage, *J. Mater. Chem. A*, 2021, **9**(21), 12606–12611.
22 B. K. Chakrabarti, M. Ouyang, B. Alkhateab, J. Rubio-Garcia, K. B. Dönmez, Z. Çobandede, R. Afshar Ghotli, S. H. Soytaş, M. K. Bayazıt, Y. S. Hajimolana, P. Kazempoor, M. Gençten, C. T. J. Low and N. P. Brandon, Enhancement in the performance of a vanadium-manganese redox flow battery using electrospun carbon metal-based electrode catalysts, *Mater. Res. Bull.*, 2025, **182**, 113140.
23 J. F. Lei, Y. X. Yao, Y. Q. Huang and Y. C. Lu, A Highly Reversible Low-Cost Aqueous Sulfur-Manganese Redox Flow Battery, *ACS Energy Lett.*, 2022, **8**(1), 429–435.
24 Y.-R. Dong, H. Kaku, K. Hanafusa, K. Moriuchi and T. Shigematsu, A Novel Titanium/Manganese Redox Flow Battery, *ECS Trans.*, 2015, **69**(18), 59.

25 K. Amini and M. D. Pritzker, Life-cycle analysis of zinc-cerium redox flow batteries, *Electrochim. Acta*, 2020, **356**, 136785.
26 Z. Na, S. Xu, D. Yin and L. Wang, A cerium–lead redox flow battery system employing supporting electrolyte of methanesulfonic acid, *J. Power Sources*, 2015, **295**, 28–32.
27 K. Amini and M. D. Pritzker, Improvement of zinc-cerium redox flow batteries using mixed methanesulfonate-chloride negative electrolyte, *Appl. Energy*, 2019, **255**, 113894.
28 Y. Wu, L. Zhou, Y. Xie, Y. Lai, S. Fu, X. Kang, W. Shi, J. Li, X. Zhang, K. Hu, H. Zhang and T. Qi, A green europium-cerium redox flow battery with ultrahigh voltage and high performance, *Chem. Eng. J.*, 2024, **500**, 157189.
29 N. Kocyigit, M. Gencten, M. Sahin and Y. Sahin, A novel electrolytes for redox flow batteries: Cerium and chromium couples in aqueous system, *Int. J. Energy Res.*, 2021, **45**(11), 16176–16188.
30 S. I. U. Ahmed, M. Shahid and S. Sankarasubramanian, Aqueous titanium redox flow batteries—State-of-the-art and future potential, *Front. Energy Res.*, 2022, **10**, 1021201.
31 K. Gong, X. Ma, K. M. Conforti, K. J. Kuttler, J. B. Grunewald, K. L. Yeager, M. Z. Bazant, S. Gu and Y. Yan, A zinc–iron redox-flow battery under $100 per kW h of system capital cost, *Energy Environ. Sci.*, 2015, **8**(10), 2941–2945.
32 K. S. K. Chivukula and Y. Zhao, Next-generation vanadium redox flow batteries: harnessing ionic liquids for enhanced performance, *RSC Adv.*, 2025, **15**(31), 25310–25321.
33 M. Ding, X. Ling, D. Yuan, Y. Cheng, C. Wu, Z. S. Chao, L. Sun, C. Yan and C. Jia, SPEEK Membrane of Ultrahigh Stability Enhanced by Functionalized Carbon Nanotubes for Vanadium Redox Flow Battery, *Front. Chem.*, 2018, **6**, 286.
34 Z. Yuan, X. Li, J. Hu, W. Xu, J. Cao and H. Zhang, Degradation mechanism of sulfonated poly(ether ether ketone) (SPEEK) ion exchange membranes under vanadium flow battery medium, *Phys. Chem. Chem. Phys.*, 2014, **16**(37), 19841–19847.
35 S. Kim, T. B. Tighe, B. Schwenzer, J. Yan, J. Zhang, J. Liu, Z. Yang and M. A. Hickner, Chemical and mechanical degradation of sulfonated poly(sulfone) membranes in vanadium redox flow batteries, *J. Appl. Electrochem.*, 2011, **41**(10), 1201–1213.
36 K. S. K. Chivukula, Y. Zhao and A. Novel, Vanadium–Titanium Redox Flow Battery with Enhanced Electrochemical Performance & Greener Alternative, *ChemElectroChem*, 2026, **13**(1), e202500441.